PROPAGATION OF LIGHT IN DISORDERED SEMICONDUCTOR MATERIALS

AD LAGENDIJK , JAIME GOMEZ RIVAS , ARNOUT IMHOF ,
FRANK J.P. SCHUURMANS AND RUDOLF SPRIK
van der Waals-Zeeman Institute, University of Amsterdam,
Valckenierstraat 65, 1018 XE Amsterdam, The Netherlands

1. Introduction

The analogy between the propagation of electron waves and classical waves has led to a revival in the research of the transport of light in disordered scattering systems [1]. The first indications of the role of interference in multiple scattering has been indicated in experiments on enhanced backscattering in the late 1980's [2]. Over the past decade many studies have been performed to characterize and understand this intricate interplay of scattering and interference [3]. The improved understanding of the optical systems stimulated the studies of the propagation of waves in disordered systems in general and applications in e.g. the field of medical imaging [4].

The 'holy grail' has been to observe the optical analogue of Anderson localization in electronic systems [5]. Anderson localization refers to an inhibition of the wave propagation in disordered scattering systems due to interference. Localization is essentially a wave phenomenon and it should hold for all kinds of waves i.e. electrons, electromagnetic and acoustic waves [6]. For isotropic scatterers Anderson localization is established if $kl_s \sim 1$, where k is the wave vector in the medium and l_s is the scattering mean free path, or the average length that the wave propagates in between two elastic collisions. The transition between extended and localized states occurs when $kl_s < 1$. This is known as the Ioffe-Regel criterion for localization [7]. To approach the Ioffe-Regel criterion, l_s can be reduced by using scatterers with a high refractive index, n, and an optimal size where the scattering cross-section is a maximum.

Experimental difficulties in realizing a random medium where the optical absorption is low enough and the light scattering is efficient enough to induce localization has been the reason why, for a long time, only mi-

C.M. Soukoulis (ed.), Photonic Crystals and Light Localization in the 21st Century, 447-473.

crowave localization was realized [8]. In this experiment the absorption is large and, therefore, complicates the interpretation of the results. Recently, near-infrared localization in GaAs powders was observed [9]. However, the validity of these measurements has been questioned by the possibility of absorption [10].

To achieve localization the parameter kl_s needs to be reduced. The light wavevector, k, is defined as $k = \frac{2\pi n_e}{\lambda}$ where λ is the wavelength and n_e is the effective refractive index of the disordered medium. The scattering mean free path, l_s, is given in first approximation by $l_s \sim \frac{1}{\rho\sigma_s}$, where ρ is the density of scatterers and σ_s their scattering cross section. The scattering cross section depends on the size of the scatterers relative to λ and on the refractive index contrast between the scatterers (n) and the surrounding medium (n_0), $m = \frac{n}{n_0}$, being larger for higher values of m.

Contrary to electronic systems, for light it is not possible to reach the localization transition ($kl_s \approx 1$) just by reducing k. In the Rayleigh scattering limit or when $\lambda \gg r$, where r is the radius of the scatterers, σ_s is proportional to λ^{-4} and therefore $kl_s \propto \lambda^3$. In this limit a reduction of k by increasing the light wavelength will give rise to an increase of the localization parameter. In the opposite limit or the geometric optics limit, $\lambda \ll r$, the scattering cross section equals $2\pi r^2$ and $kl_s \propto \frac{1}{\lambda r^2}$. Thus reducing λ will not help either to approach the localization transition. Therefore, localization of light will only be possible at an intermediate wavelength window where the scattering cross section is maximal, that is, when the size of the scatterers is of the order of the wavelength, $\lambda \sim r$. Even then the refractive index contrast needs to be high enough to reach the localization transition.

Here we present an overview of our recent measurements on Si [11] and Ge powders and on a unique form of porous GaP[12, 13]. We will discuss the method to observe deviations from diffusive transport and the occurrence of localization. Important are good characterization of the materials by a systematic study of static and dynamical properties. We will discusss the role of residual absorption, effective refractive index on internal reflection and topology of the sample.

2. Disordered semiconductor systems

Much experimental work has been done on powders of TiO_2 [14, 15, 16]. TiO_2 is the dielectric with the highest refractive index in the visible, $n = 2.7$, and, although the TiO_2 samples were strongly scattering, the lowest value of the localization parameter was still far from the transition ($kl_s \approx 6$). Some semiconductors like Ge, GaAs, Si and GaP have larger refractive indices than TiO_2 and very low absorption for $\lambda > \lambda_{\text{gap}}$, where λ_{gap} is the wavelength of the semiconductor energy band gap. In table 1 we list, for

Material	n	$\lambda_{\rm gap}$ (nm)	Reported kl_s (at λ)	Structure	Reference
GaAs	3.5	890	< 1 (1.067 μm)	powder	[9]
GaP	3.2	550	~ 2 (0.633 μm)	porous	[12]
Ge	4.1	1850	~ 3 (2 μm)	powder	[24]
Si	3.5	1100	~ 3.5 (6.5 μm)	powder	[11]
TiO_2	2.7	> 300	~ 7 (0.633 μm)	powder	[15]

TABLE 1. refractive index, n, and wavelength of the energy band gap, $\lambda_{\rm gap}$, of several semiconductors. The lowest reported value of the localization parameter, kl_s, and the structure of the samples are also listed.

these semiconductors, the refractive index n and $\lambda_{\rm gap}$. Therefore, they are good candidates to prepare a material where light is localized. We have also included in table 1 the lowest measured value of kl_s. Strong localization of light ($kl_s < 1$) was first and solely reported in GaAs powders [9]. However, an alternative explanation for these measurements was proposed in terms of classical light diffusion and optical absorption [10]. It was clear that a thorough characterization of these novel materials was necessary.

We have prepared samples with different structure, powders and porous materials, as it is indicated in table 1. In the following we describe the preparation method for the different samples. The starting material of the Si samples was commercially available powder of high purity Si particles (Cerac S-1049) with sizes ranging from a few hundred nanometers to about 40 μm. To reduce the polydispersity in the particle size we suspended the particles in spectroscopic grade chloroform and we let them sediment for 5 minutes. Only the particles that did not sediment were used in the experiments. Fig. 1(a) is an scanning electron microscopy (SEM) image of these particles. We can see that the Si particles are rounded and that they tend to aggregate into clusters. Considering the clusters as single particles, the average particle radius is $\bar{r} = 690 \pm 410$ nm. Layers of Si powder with different thickness were made by putting a few drops of the suspension on CaF_2 substrates and letting the chloroform evaporate [11].

The Ge samples were prepared starting from bulk pieces of Ge that were gently milled. Sedimentation of the biggest particles was necessary in order to keep the milling time and intensity as low as possible. A SEM image of the resulting Ge particles is shown in Fig. 1(b). As may be noticed, the Ge particles do not form clusters and their shape is different from that of the Si particles. The average Ge particle size is $\bar{r} = 980 \pm 680$ nm. The still high polydispersity of the Si and Ge particles has serious disadvantages, since

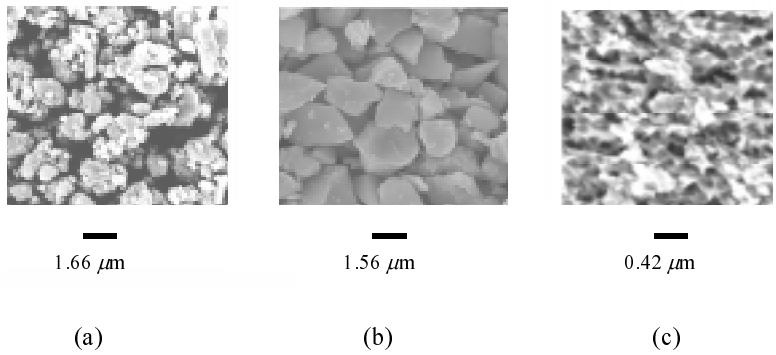

Figure 1. Scanning electron microscope images of disordered semiconductor samples. (a) Si powder, (b) Ge powder and (c) porous GaP (PA-GaP).

the average scattering cross section becomes lower as the polydispersity increases. Layers of Ge particles were made in a similar way as for Si, for which we suspended the particles in spectroscopic grade methanol.

The GaP samples are porous or sponge-like layers of GaP. The porous structure was formed by anodic etching of n-type single crystalline GaP wafers [12]. Samples of two types were made: anodically etched GaP (A-GaP) with a porosity of 35% and photoanodically etched GaP (PA-GaP) with a porosity of 50%. The PA-GaP samples were prepared by further etching A-GaP using homogeneous photo-assisted etching [12]. The resulting samples are layers of different thickness of porous GaP on bulk GaP wafers or substrates. Figure 1(c) is a SEM image of PA-GaP sample. The average pore size in the A-GaP samples is estimated to be $\bar{r} = 92 \pm 30$ nm while for the PA-GaP samples $\bar{r} = 132 \pm 30$ nm.

Finally, it is necessary to mention that the structure of the samples will play an important role in its scattering properties. For instance, it has been demostrated that the values of kl_s for the inverse structure of air spheres in high dielectric materials (porous material) is lower that those for the direct structure of spheres of high dielectric material in air (powder) [17]. Also the shape of the particles or pores will influence the scattering.

3. Static characterization

In this section we describe the static measurements. From these measurements important sample parameters as l_s, l, L_a and n_e are obtained. The optical absorption in the medium is characterized by the absorption lenght, L_a. The transport mean free path, l, is defined as the distance over which the direction of propagation of the wave is randomized and vanishes in the localization regime. The scattering mean free path, l_s, constitutes a measure of the disorder quantified by the localization parameter. Let us briefly describe the propagation of light in disordered scattering media. In the weak scattering limit, $kl_s \gg 1$, the propagation of light is well described by the diffusion equation [18]. The diffusion approximation neglects the interference of waves propagating along different paths since, on average, this interference cancels out. The light diffuses in the medium with a diffusion constant given by

$$D_B = \frac{v_e l_B}{3}, \tag{1}$$

where v_e is the energy velocity and l_B the Boltzmann mean free path, defined as the transport mean free path in the absence of interference. If a sample is illuminated, the source of diffuse radiation is given by the light scattered out of the incident or coherent beam. The incident beam decays as $\exp(-z/l_s)$ where z is the depth in the sample. The diffuse total transmission, defined as the transmitted light flux normalized by the incident flux, can be calculated by solving the diffusion equation with the proper boundary conditions. The boundary conditions are determined by considering that the diffuse fluxes entering the sample are due to a finite boundary reflectivity [19, 20]. This reflectivity arises from the refractive index mismatch between the sample and the outside world. The total transmission will, therefore, depend on the boundary reflectivities by means of the so-called extrapolation factors τ_1 and τ_2 where the index 1 refers to the interface where the incident beam enters the sample and the index 2 to the opposite interface. The extrapolation factors τ_1 and τ_2 are given by [20]

$$\tau_1 = \frac{2}{3}\left(\frac{1+\overline{R}_1}{1-\overline{R}_1}\right), \tag{2}$$

and a similar expression for τ_2. Where $\overline{R}_1$ is the polarization and angular averaged reflectivity of the boundary. The extrapolation lengths z_1 and z_2 are defined as the extrapolation factors times the transport mean free path. Thus, in the weak scattering limit we have $z_1 = \tau_1 l_B$ and $z_2 = \tau_2 l_B$.

In the case of non-absorbing samples, represented by the condition $L_a > L$, where L_a is the optical absorption length and L is the sample thickness,

the total transmission is

$$T = \frac{l_B + z_1}{L + z_1 + z_2}. \tag{3}$$

The total transmission decays as the inverse of the sample thickness, similarly to Ohm's law for the electronic conductance. If significant absorption is present in the samples, $L_a < L$, the total transmission decays exponentially with sample thickness,

$$T = \frac{2L_a(l_B + z_1)}{L_a^2 + (z_1 + z_2)L_a + z_1 z_2} \exp\left(-\frac{L}{L_a}\right). \tag{4}$$

As the localization transition is approached the diffusion constant is renormalized by wave interference, which, according to the scaling theory of localization [21], is given by

$$\frac{D}{D_B} = \frac{l}{l_B} = l_B \left(\frac{1}{\xi_0} + \frac{1}{L_a} + \frac{1}{L}\right), \tag{5}$$

where the coherence length ξ_0 represents the length over which the interference is important. At the localization transition ξ_0 diverges, thus in an infinite and non-absorbing medium D and l vanish. At the transition the transport of light is inhibited.

In a non-absorbing medium in the strong localization regime ($kl_s < 1$) the total transmission is

$$T \propto \exp\left(-\frac{L}{L_{loc}}\right), \tag{6}$$

and the wave is spatially localized on length scales given by the localization length, L_{loc}. Notice that the equal dependence of the transmission on the sample thickness in the case of classical light diffusion in an absorbing medium (Eq. 4) and in the case of strong localization in a non-absorbing medium (Eq. 6) greatly complicates the analysis of these measurements. However, optical absorption is not necessarily a disadvantage. The role of absorption in the localization process has been never experimentally investigated and this can not be done in electronic systems since the number of electrons is conserved.

In the following we describe the static measurements that we have performed on disordered semiconductors materials. The simplest experiment consists in measuring the decay of intensity of the coherent beam sent through the samples. The transmitted fraction of the coherent beam, T_{coh}, is given by the expression

$$T_{\mathrm{coh}} = \exp(-L/l_s). \tag{7}$$

Sample	l_s (μm) at $\lambda = 740$ nm	n_e	kl_s
A-GaP	0.4 ± 0.1	~ 2.0	6.8
PA-GaP	0.25 ± 0.05	1.5 ± 0.2	3.2

TABLE 2. Scattering mean free path, l_s, effective refractive index, n_e, and localization parameter, kl_s, of A-GaP and PA-GaP samples.

To measure $T_{\rm coh}$ one can place a detector at a long distance behind the sample and in the direction of the incident beam. By doing this the detected diffuse transmission is negligible compared to the coherent transmitted fraction. Unfortunately due to the exponential decay of $T_{\rm coh}$ these measurements can only be done for thin samples and an intense light source is needed. To avoid semiconductor band gap absorption the wavelength must be greater than $\lambda_{\rm gap}$. For the GaP samples we used as radiation source a mode-locked Ti:Sapphire laser (Spectra Physics Tsunami) at a central wavelength of 740 nm. The values of l_s in the GaP samples at $\lambda = 740$ nm obtained from the measurement of $T_{\rm coh}$ are summarized in table 2. The scattering mean free path is shorter in PA-GaP due to its higher porosity.

The band gap of Ge is at $\lambda = 1.85$ μm, therefore we used as radiation source a Free Electron Laser (FELIX, Rijnhuizen, The Netherlands), which could be easily tuned in the near and mid-infrared (from 4.5 to 200 μm) [1]. We measured $T_{\rm coh}$ at $\lambda = 5$, 6.5, 7 and 8 μm. In the inset of Fig. 2 we plot the measurements at $\lambda = 8$ μm as function of the sample thickness and a fit to Eq. 7, from which we obtain $l_s = 3.8 \pm 0.2$ μm. Figure 2 shows the wavelength dependance of l_s. As expected l_s increases as λ becomes larger. This is due to the reduction of the scattering cross section when the wavelength becomes significantly larger than the scatterers size.

To obtain the localization parameter, $k = \frac{2\pi n_e}{\lambda} l_s$, we still need to know the effective refractive index of the samples, n_e. By measuring the angular dependence of the diffuse transmission it is possible to obtain this important parameter. This is because the angular distribution of the transmitted light is affected by the refractive index mismatch between the sample and the exterior, but not by l or l_s. Defining θ_i as the angle at which the diffuse light is incident on the interior side of the sample boundary with respect to the sample surface normal, and θ_e as the angle at which the light exits the sample (θ_i and θ_e are related by Snell's law), the transmission probability

[1]The experiments at FELIX where done in collaboration with C.W. Rella and L.D. Noordam from the FOM-Institute for Atomic and Molecular Physics (AMOLF, The Netherlands).

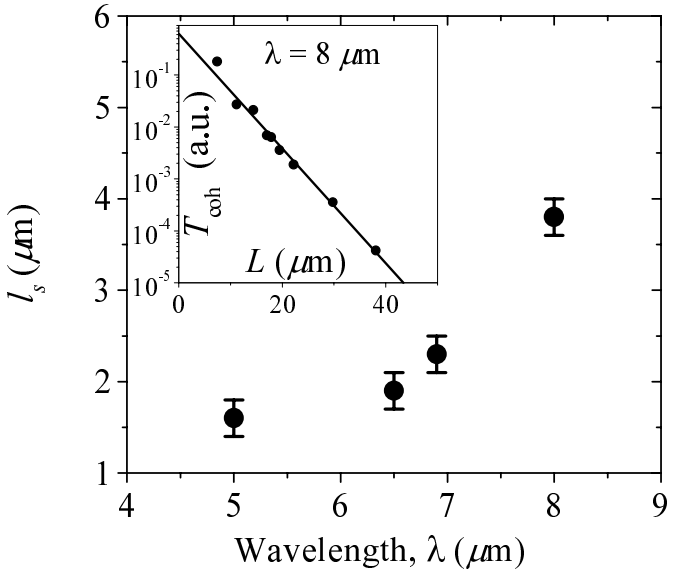

Figure 2. Wavelength dependence of the scattering mean free path, l_s, in Ge powder samples. Inset: measurements of the transmitted fraction of the coherent beam in the Ge samples as function of the sample thickness, L, for $\lambda = 8$ μm. The solid line is an fit to $T_{\rm coh} = \exp(-L/l_s)$, with and scattering mean free path $l_s = 3.8 \pm 0.2$ μm.

at an angle θ_e, $P(\theta_e)$, is given by [22]

$$\frac{P(\theta_e)}{\cos\theta_e} \propto (\tau_2 + \cos\theta_i)(1 - R_2(\theta_i)) \tag{8}$$

where $R_2(\theta_i)$ is the Fresnel reflection coefficient at an incidence angle θ_i on interface 2. As $R_2(\theta_i)$ and τ_2 are functions of the refractive index contrast between the sample and the outside medium, it is possible to obtain n_e from the measurements $P(\theta_e)$. The measurements of $P(\theta_e)$ are done by rotating a detector around the sample. In Fig. 3 we plot as squares $P(\theta_e)/\cos(\theta_e)$ as a function of $\cos(\theta_e)$ for a 10 μm thick PA-GaP sample. By placing a polarizer between the sample and the detector we also measured the s and p-polarization components (triangles and circles in Fig. 3). The three measurements are fitted to Eq. 8 with the appropriate Fresnel reflection coefficients and with n_e as single free fitting parameter obtaining $n_e = 1.5 \pm 0.2$. For the A-GaP samples it is not possible to obtain n_e from the measurements of $P(\theta_e)$ because these samples have a thin low-porosity overlayer of 0.1-0.2 μm. As $P(\theta_e)$ is determined by the sample interface characteristics, for A-GaP samples these measurements are affected by the

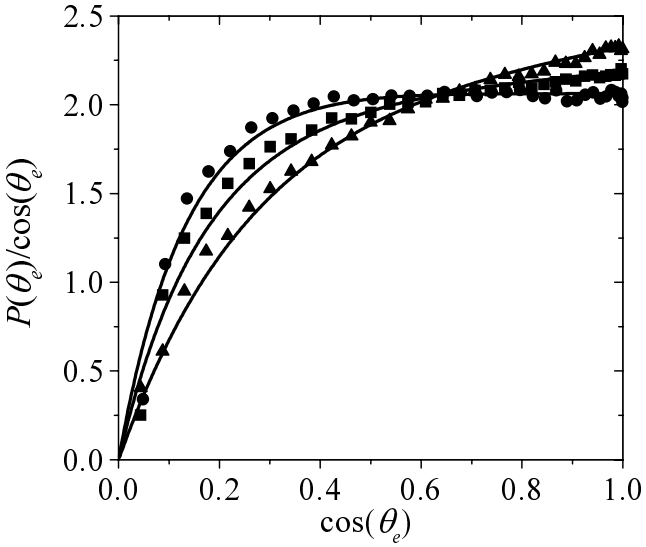

Figure 3. Transmission probability of a PA-GaP as a function of $\cos(\theta_e)$, where θ_e is the transmission angle with respect to the sample surface normal. The triangles and circles are the measurements for s and p-polarization detection while the squares correspond to unpolarized detection. The solid lines represent fits to classical diffusion theory from which the effective refractive index of the samples, $n_e = 1.5 \pm 0.2$, is obtained.

thin overlayer, making it impossible to infer from them a bulk property as n_e. Photo-assisted etching of the A-GaP to form PA-GaP removes the overlayer. However, we can estimate n_e knowing their porosity (35%). A good estimate of n_e is given by the Maxwell-Garnett effective refractive index [23], which in the case of A-GaP gives $n_e \sim 2.0$. In table 2 the measured value of n_e for PA-GaP and the estimated one for A-GaP are listed, together with the localization parameter. PA-GaP is very close to the localization transition, $kl_s = 3.2$, being the strongest scattering material of visible light to date.

By weighing the Ge powder samples we have estimated a material volume fraction of $\sim$ 40. The corresponding value of the Maxwell-Garnett effective refractive index is $n_e \sim 1.6$. The localization parameter as a function of λ for the Ge samples is plotted in Fig. 4. The relatively high value of the localization parameter, regarding the high refractive index of Ge, and the nearly constant value of the localization parameter with λ can be understood in terms of the high polydispersity in the Ge particle size. As it is discussed in Ref.[11], due to the polydispersity the resonances in σ_s are

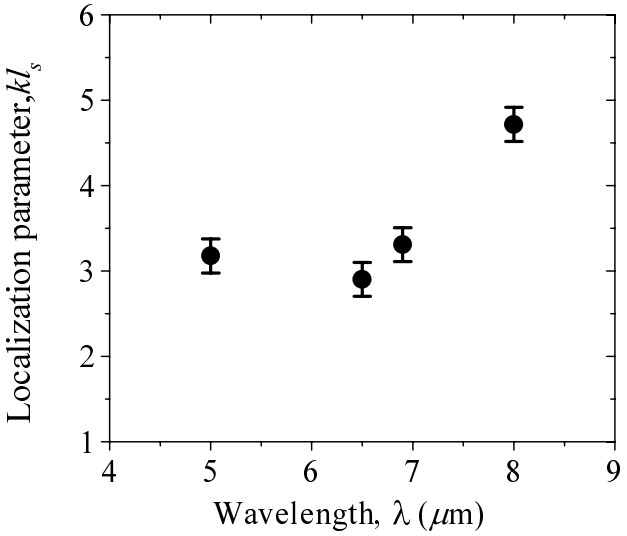

Figure 4. Wavelength dependence of the localization parameter in the Ge powder samples.

smoothed out and the average scattering cross section becomes in general larger than in a monodisperse system. Therefore to achieve localization in the Ge powder samples the polydispersity needs to be further reduced by, for instance, selective sedimentation.

The transport mean free path can be obtained from the total transmission measurements. The samples were mounted at the input of a $BaSO_4$ coated integrating sphere. The integrating sphere collected the diffuse transmitted light that was detected with a detector placed at the output port. To obtain an absolute value of the total transmission the measurements were normalized by the incident intensity. In all the samples (GaP, Ge and Si) the incoming beam was incident on the air-sample interface and the transmitted light exited the sample through the sample-substrate interface. For simplicity, in the determination of τ_2 we have not considered the reflections at the interface substrate-air. These reflections give rise to a larger value of τ_2. However, the total transmission through thick samples ($L \gg l$) is almost insensitive to the value of τ_2, as is clear from Eq. 3, and an underestimate of τ_2 will not affect the values of l. The inverse of the total transmission of the GaP samples, at $\lambda = 740$ nm, versus the sample thickness is plotted in Fig. 5. The circles are the measurement of A-GaP, while the squares corre-

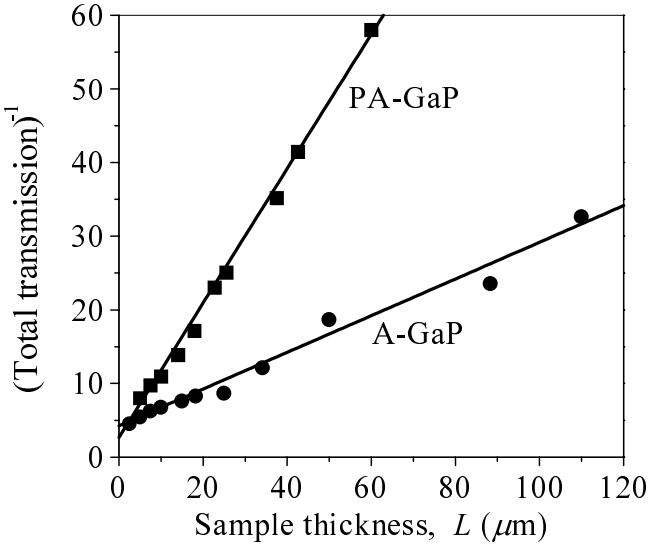

Figure 5. Inverse of the total transmission versus the sample thickeness, L, for PA-GaP (squares) and A-GaP (circles) samples. The solid lines are fits using the diffusion theory.

spond to PA-GaP. The linear dependence of T^{-1} on L is a clear signature that absorption is negligible, that is $L_a > 110$ μm in the A-GaP samples and $L_a > 60$ μm in the PA-GaP samples. With the values of n_e (table 2) and Eq. 2 the extrapolation factor τ_1 can be calculated, being $\tau_1 = 5.14$ for A-GaP and $\tau_1 = 2.42$ for PA-GaP. The solid lines in Fig. 5 are fits using Eq. 3. From the slope of these lines and with τ_1 we obtain $l = 0.65 \pm 0.03$ μm for A-GaP and $l = 0.32 \pm 0.04$ μm for PA-GaP. These values of l are slightly larger than l_s, which means that the scatterers are not fully isotropic.

We have also measured the total transmission of the Ge samples in the mid-infrared using the free electron laser [24], but lets here discuss the measurements on the Si samples. For the Si powder samples a tungsten halogen lamp was used as a light source and the total transmission spectra were measured with a Fourier transform infrared spectrometer (BioRad FTS-60A). The spectrum of a 57.8 μm thick sample is shown in the inset of Fig. 6. In Fig. 6 we plot the total transmission of the Si samples as a function of their thickness, L, for $\lambda = 1.4$ μm (circles) and 2.5 μm (squares). From the Si volume fraction (~ 40 %), n_e is estimated to be ~ 1.5 and the extrapolation factors of the interfaces sample-air, τ_1, and sample-substrate, τ_2, are ~ 2.4 and ~ 0.78 respectively. The solid lines in Fig. 6 represent

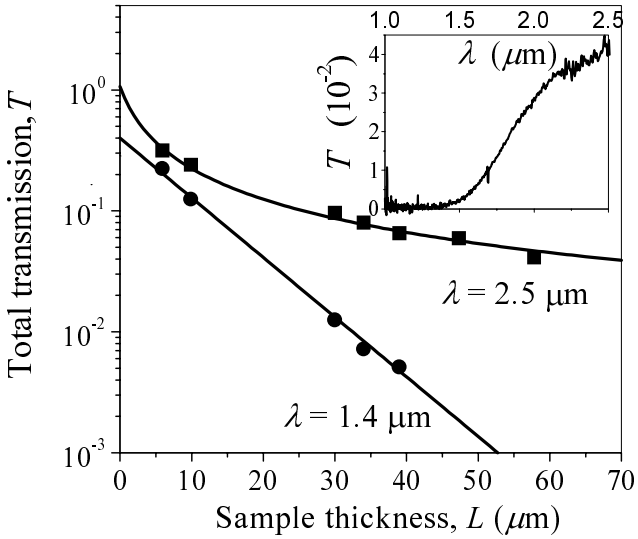

Figure 6. Total transmission through Si powders as a function of the sample thickness, L, for $\lambda = 1.4$ μm and $\lambda = 2.5$ μm. The solid lines are fits using classical diffusion theory. The inset shows the total transmission spectrum of a $L = 57.8$ μm sample.

fits to the measurements using classical diffusion theory (Eqs. 3 and 4). At $\lambda = 2.5$ μm we find $l = 0.83\pm\ 0.09$ μm and $L_a > 60$ μm, while at $\lambda = 1.4$ μm, $l = 0.56 \pm 0.05$ μm and $L_a = 8.8 \pm 0.1$ μm.

The wavelength dependence of L_a is plotted in Fig. 7. The strong absorption at $\lambda < 2.0$ μm is due to strain in the Si lattice structure, which creates band gap tails that increase considerably the absorption at sub-band gap energies with respect to the strain-free material. We have confirmed the presence of strain by means of X-ray diffraction.

The dots in Fig. 8 represent the transport mean free path in the Si powder samples as a function of the wavelength. In collaboration with C.M. Soukoulis and K. Busch we have calculated the transport mean free path in the Si samples using the Energy Density Coherent Potential Approximation (EDCPA) [23, 25]. For the calculation we considered spherical and isotropic ($l = l_s$) scatterers. The dotted line in Fig. 8 is the calculated l of a monodisperse system of Si spheres with a volume fraction of 40% and a sphere radius equal to $\bar{r}$. The solid line in the same figure represents the averaged l over the particle size polydispersity. The resonances in l are smoothed out due to the polydispersity and in general l becomes larger. A

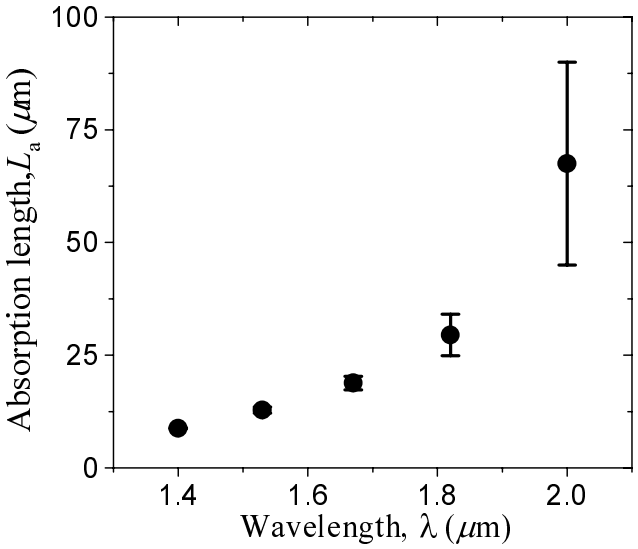

Figure 7. Absorption length, L_a, in Si powders as a function of the wavelength, λ.

good qualitative agreement is found between experiments and theory. The small quantitative difference can be attributed to the non-spherical shape of the Si particles and the ambiguous definition of the $\bar{r}$ due to the particle clustering. Assuming that the scatterers are isotropic and that $n_e = 1.5$ (Maxwell Garnett refractive index of the samples), we find a nearly constant value of $kl_s \sim 3.5$ in the studied wavelength range. As discussed for Ge, a reduction in the polydispersity of the Si particles will give rise to a lower value of the localization parameter.

We have also done enhanced backscattering (EBS) measurements on the GaP samples [13]. With these measurements we can check the consistency of the total transmission measurements and look for localization effects. We have measured the EBS of A-GaP and PA-GaP using the off-centered rotation technique [26]. The EBS measurements at $\lambda = 685$ nm are shown in Fig. 9. From the width of the cones the values of the transport mean free path can be inferred. For A-GaP (narrow cone) we find $l = 0.58 \pm 0.05$ μm, while for PA-GaP (wide cone) $l = 0.23 \pm 0.03$ μm, thus in good agreement with the total transmission measurements. The scattering efficiency can be reduced by decreasing the refractive index contrast in the samples. This can be achieved by filling the air voids in the samples with a non-absorbing liquid. In Fig. 10 the EBS of a PA-GaP sample filled with 1-dodecanol

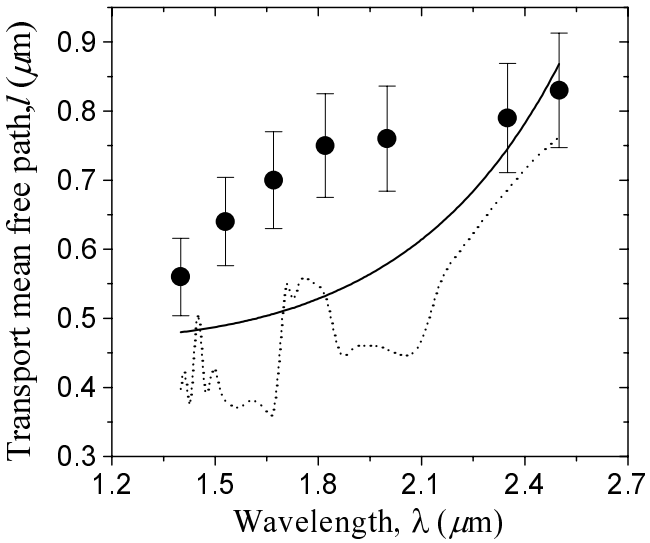

Figure 8. Transport mean free path of light, l, in the Si powder samples versus the wavelength, λ. The dotted line is l, calculated using the energy density coherent potential approximation, of a system of 40% by volume of Si spheres with a size equal to the average Si particle size. The solid line is the calculated l considering the polydispersity of the particles.

($n \sim 1.44$ and no absorption at $\lambda = 685$ nm) together with the EBS of the same non-filled sample are shown. The cone of the non-filled sample is a factor 2.1 ± 0.1 broader than the filled one, corresponding to an increase of the transport mean free path. Of special interest is the rounding of the cone top, $\triangle\Theta_R$, as is shown in the inset of Fig. 10. Within the classical diffusion approximation this rounding can be due to two factors: absorption and the finite size of the samples. The expression relating the rounding with the absorption length and the sample thickness can be derived to be [13]

$$\triangle\Theta_R = \frac{1}{kL_a} \coth\left(\frac{L_e}{L_a}\right), \tag{9}$$

where $L_e = L + z_1 + z_2$ is the effective sample thickness. In the absence of absorption, $L \ll L_a$, Eq. 9 reduces to

$$\triangle\Theta_R = \frac{1}{kL_e}. \tag{10}$$

To investigate the mechanisms of the cone rounding, we measured the EBS for various sample thicknesses. The cone rounding of A-GaP, PA-GaP and

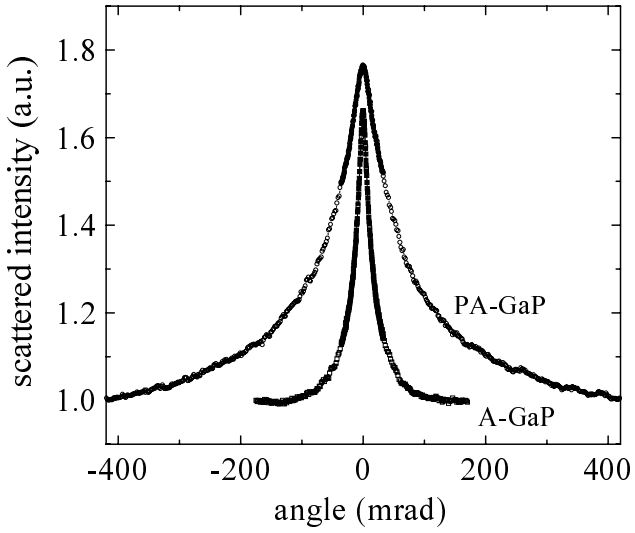

Figure 9. Enhanced backscattering of A-GaP and PA-GaP.

PA-GaP filled with 1-dodecanol are shown in Fig. 11 as open squares, open circles and filled triangles respectively as a function of $(kL_e)^{-1}$. Clearly, the cone rounding of A-GaP and filled PA-GaP follow Eq. 10. Absorption plays no role for these two types of samples and the rounding can be fully described in terms of the finite sample size. In contrast, the cone rounding of PA-GaP does not tend to zero for thick samples. If the measurements are fitted with Eq. 9 we find $L_a = 33 \pm 2$ μm. This contradicts the total transmission measurements from which we concluded that $L_a > 60$ μm. Moreover, if absorption is responsible for the rounding of the cone of PA-GaP, an extra rounding in the cone of the filled samples should also be apparent, which clearly is not the case. The extra rounding is only observed in the strongest scattering material which is the closest to the localization transition. It is expected that interference effects due to the proximity of the localization transition change the EBS cone shape. This change should be more significant in the cone cusp, since only at Θ close to 0 long paths contribute to the EBS. In particular it has been demonstrated that due to localization the cone cusp becomes rounded [27], similarly to our observation in PA-GaP.

Finally, we should mention that by filling the samples with non-absorbing liquids it is possible to verify if an exponentially decreasing total transmis-

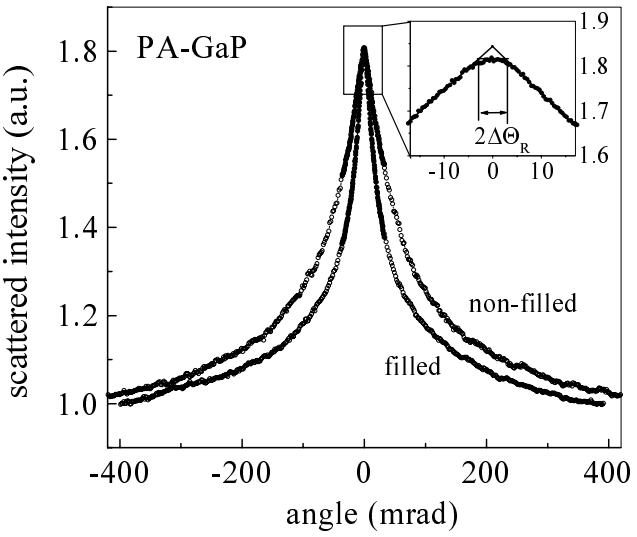

Figure 10. Enhanced backscattering of a PA-GaP sample with the air voids filled with 1-dodecanol and the same sample with non-filled pores. The inset is the a magnification of the cone top of the filled sample where the rounding of the cusp, $\triangle\Theta_R$, is visible.

sion with L is due to strong localization (Eq. 6) or if absorption needs to be considered. We have realized this experiment in Ge samples close to the band gap as is shown in Ref. [28].

4. Dynamic characterization

In this section we describe an interferometric technique for measuring time-resolved light transmission by random scattering media [29]. In this technique an incident ultrashort laser pulse is interfered with light transmitted by the medium. Since diffusely scattered light is incoherent an interferogram is obtained only if the scattered light is limited to a single (or just a few) coherence area, or speckle spot, at a time. Properties of light transport are then determined by repeating the measurement for many different configurations of scatterers and taking the appropriate average. This way one can measure the diffusion coefficient D, and with it the energy velocity v_e [16]. Due to the high dynamic range of the technique the decay rate $1/t_d \propto D/L^2$ of the tail of the diffusely transmitted pulse can be accurately determined. We use this to search for deviations that are expected to occur when the localization threshold is reached and D becomes thickness-dependent. For

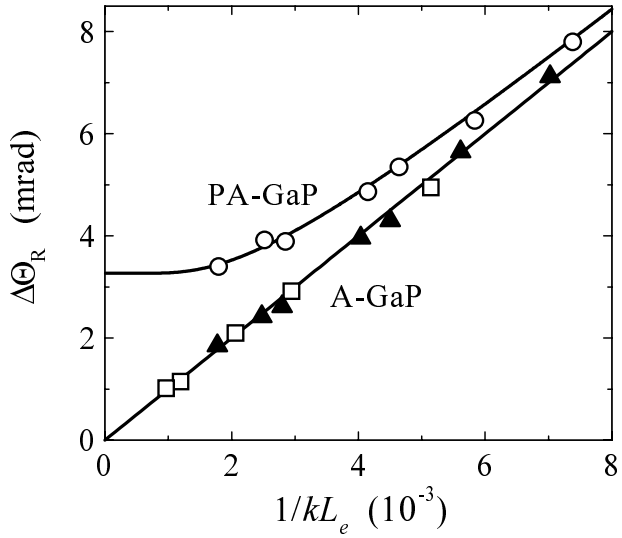

Figure 11. Cone roundings, $\triangle\Theta_R$, of A-GaP (open squares), PA-GaP (open circles), and PA-GaP filled with 1-dodecanol (filled triangles) as a function of the inverse of the effective sample thickness. The solid straight line is the theoretical prediction assuming a negligible absorption, Eq. 10 , using no adjustable parameters. PA-GaP shows an extra rounding for thick samples. The measurements are fitted to Eq. 9 with $L_a = 33 \pm 2$ μm. This absorption length is not consistent with the total transmission measurements.

example, near the mobility edge one expects to find $1/t_d \propto 1/L^3$ [30]. Furthermore, we will show that with our technique statistical information can be obtained on the fluctuations in the phases and amplitudes of multiply scattered light. This kind of dynamical information was hitherto unavailable for light, and makes possible a more detailed dynamical study of light propagation in strongly scattering media. Results are presented for samples of A-GaP.

In these experiments we used bandwidth-limited ultrashort pulses ($\sim$100 fs) from a Ti:Sapphire laser (Spectra Physics Tsunami) at 740 nm, with a repetition rate of 82 MHz. The spectral bandwidth of the pulses is about 1% of the central frequency, so that the mean free paths can be considered constants over this range. A double-pulsed signal is obtained with a fixed Mach-Zehnder interferometer in which the reference arm is empty and the sample arm contains the scattering sample. The sample beam and reference beam which emerge from the interferometer are carefully overlapped. This produces a pair of pulses: an undisturbed pulse followed by a pulse scattered

by the sample into the forward direction. The pulse separation ΔL is the difference in the optical path lengths of the two arms of the interferometer. This beam is sent into an FTIR spectrometer (Biorad FTS-60A). The FTIR uses a scanning Michelson interferometer to obtain the field autocorrelation function of the pulse pair by scanning the time delay τ between two copies of the pair. The intensity is sampled by a PMT at a rate of 5 kHz. By this way samples are acquired every 0.27 fs in τ. The measured signal contains interference fringes whenever τ is such that two pulses overlap. This occurs if $\tau = 0$ or if $\tau = \pm\Delta L/c$, with c the speed of light. Around $\tau = 0$ the sample pulse overlaps with its own copy and so does the reference pulse. Apart from a constant background, the measured function is then the sum of the field autocorrelations of the two pulses. Around $\tau = \pm\Delta L/c$ one copy of the sample pulse overlaps with one copy of the reference pulse. This produces the cross correlation function of the incident field E_{in} and the scattered field E_{scat}:

$$C(\tau) = \frac{1}{\triangle T} \int_{-\triangle T/2}^{\triangle T/2} E_{in}^{*}(t) E_{scat}(t-\tau) dt, \tag{11}$$

which contains both *amplitude* and *phase* information on the pulse transport through the sample. $\triangle T$ is the repetition time of the laser, which is much longer than the pulse width.

The sample was placed between two identical lenses of 60 mm focal length, which are in confocal position. The first lens is used to focus the beam onto the sample in a small spot. The second lens collects the scattered light into a parallel beam which is then sent through an aperture. By moving the sample close to the common focal point the illuminated area can be reduced to about 10 μm. This increases the angular size of the speckles such that a single speckle spot can be selected in the scattered beam with the aperture. Different configurations of scatterers are produced by moving the sample in the plane perpendicular to the beam by a distance larger than the illuminated spot. Typically, 60 configurations were measured. For each configuration 50 scans were averaged to reduce noise. The power incident upon the sample was $\sim$0.1 W. Identical results were obtained when the incident power was halved, so nonlinear effects were absent.

In Fig. 12 the measured interferograms of a number of different speckles are shown. Each of these signals represents the temporal profile of the field transmitted in a different speckle spot, convoluted with the incident field. The signals are filled with fringes resulting from the rapid oscillations of the electromagnetic field. It is clear that the signal of each speckle is completely different because it consists of a unique sum of fields that have propagated along different paths, each of which has its own random amplitude and phase.

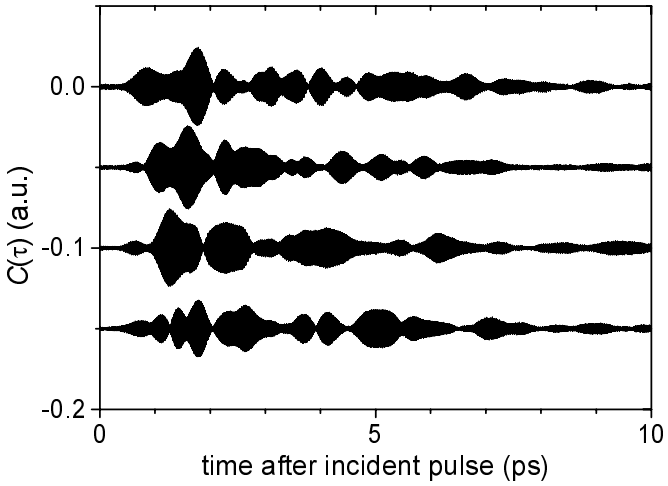

Figure 12. Interferograms from a number of different speckles measured on a sample of A-GaP of L =15 μm thickness.

The most important dynamical parameter describing propagation of light in random media is the diffusion coefficient D. The most direct way to measure it is a time resolved measurement in which a short laser pulse is incident upon the sample and one measures the time dependence of the transmitted intensity using a fast detector. This can then be compared to the prediction of diffusion theory to obtain D. Solving the diffusion equation with the proper boundary conditions for a slab of scattering material of thickness L one gets for the total transmission T [31]

$$T(t) = \frac{-2\pi D e^{-Dt/L_a^2}}{(L+z_1+z_2)^2} \sum_{n=1}^{\infty} n \quad \sin(\pi n \tfrac{l+z_1}{L+z_1+z_2}) \cos(\pi n \tfrac{L-l+z_1}{L+z_1+z_2}) \times \exp(-\tfrac{\pi^2 n^2 Dt}{(L+z_1+z_2)^2}). \tag{12}$$

Here, z_1 and z_2 are the extrapolation lengths on the incident and transmitting side of the slab, respectively. In interferometric measurements a fast detector is not needed because time is measured by the optical retardation of the interferometer. The time dependence of the transmitted intensity is obtained by squaring the measured cross correlations, and averaging over all speckles. The fringes average out because their phases are random. To

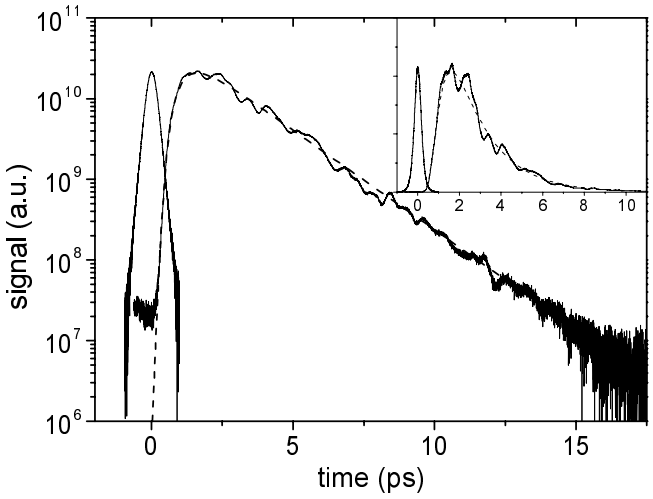

Figure 13. The diffusely transmitted pulse obtained by summing the squares of the interferograms of 60 different speckles of a sample of A-GaP of 15 μm thickness. The narrow pulse centered around the time origin is the incident pulse. The dashed line is Eq. 12 with $D = 21$ m^2/s and $L_a = \infty$. Inset: same data on a linear scale.

remove the remaining fringes the function is Fourier filtered. The result is shown in Fig. 13. The wiggles in the transmitted pulse form are due to the limited number of speckles (sixty). The time origin is found by moving the sample out of the beam and measuring the arrival time of the (now undistorted) pulse, which is also shown in Fig. 13. The semilog-plot demonstrates the high dynamic range of the measurement: An exponential decay over more than 3 orders of magnitude of the intensity is observed. This can be compared to Eq. 12 , which at long times predicts a single exponential decay with a rate $1/t_d$ given by

$$\frac{1}{t_d} = \frac{D}{L_a^2} + \frac{\pi^2 D}{(L + z_1 + z_2)^2}. \tag{13}$$

By plotting the decay rate against $1/L^2$ the validity of the diffusion equation is verified, and the values of L_a and D can be found. This is done in Fig. 14, where the expected linear relation is indeed found. From the slope we find $D = 21$ m^2/s. The intercept is zero within the experimental error, setting a lower limit on the diffuse absorption length: $L_a > 30$ μm. This means that the samples do not suffer from absorption (which was also

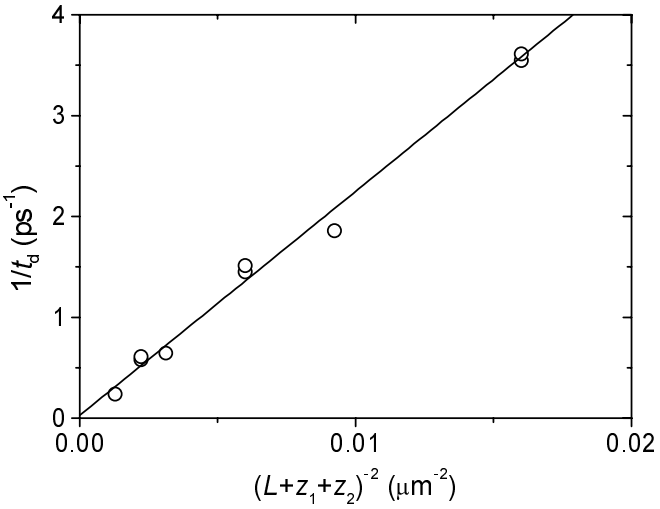

Figure 14. Decay rate of the tail of the transmitted pulse versus the inverse of the thickness squared. The solid line is a linear fit to Eq. 13.

clear from the total transmission measurements). Using only the value of D in Eq. 12 the form of the transmitted pulse is described very well, see Fig. 13. Using Eq. 1 and the value of l from the total transmission measurements an energy velocity of $0.32c$ is found, where c is the speed of light in vacuum.

An alternative way to obtain D is from dynamical speckle measurements. Using a tunable single frequency laser one can measure the intensity autocorrelation function within a single speckle spot, $C_I(\triangle\omega) = \langle \delta I(\omega)\delta I(\omega + \triangle\omega)\rangle$, where $\delta I(\omega) \equiv I(\omega) - \langle I(\omega)\rangle$. This function is related to the Fourier transform of the time dependence of the transmitted pulse [31]. The autocorrelation function of the scattered field $C_E(\triangle\omega) = \langle E(\omega)E^*(\omega+\triangle\omega)\rangle$ is similarly, and even more directly, related to the transmitted pulse shape. These functions can also be obtained from the interferometric data, as we shall see below.

Now we examine the phases and amplitudes contained in the data. The complex Fourier transform of the interferogram of a speckle, Eq. 11, gives $C(\omega) \sim E^*_{in}(\omega)E_{scat}(\omega)$. If this is divided by the Fourier transform of a reference interferogram measured without the sample, $C_0(\omega)$, the field transmission coefficient $t_{ab}(\omega)$ is obtained:

$$\frac{C(\omega)}{C_0(\omega)} = \frac{E_{scat}(\omega)}{E_{in}(\omega)} \equiv t_{ab}(\omega) \tag{14}$$

The subscripts indicate that the field transmission is measured for incident mode a and transmitted mode b. This means, for example, that the total transmission for incident mode a is obtained by summing over all transmitted speckles, $T_a = \sum_b |t_{ab}|^2$. The field transmission contains real and imaginary parts. The modulus of $t_{ab}(\omega)$ is plotted in Fig. 15 for a particular speckle of the 15 μm A-GaP sample. Also the phase ϕ_{ab} contains fluctuations. These are superposed on a linear increase with frequency, given by ωt, where t is the average traversal time of the waves. In Fig. 15, we therefore plotted the frequency derivative of the phase, $d\phi_{ab}/d\omega$. This quantity can be interpreted as the travel time of a wave of frequency ω through the sample. Indeed, in a homogeneous sample this phase derivative is equal to the inverse of the group velocity [32]. In a scattering sample, however, there are large fluctuations around a well-defined average, which is proportional to the inverse of the energy velocity. The average value of the phase derivative in this sample is equal to 2.32 ps and corresponds to the average traversal time $t_{av} = (L + z_1 + z_2)^2/6D$. For this sample we find $D = 23$ m^2/s, which agrees well with the value found from the decay of the tail of the transmitted intensity. It is also a clear from Fig. 15 that the amplitude and phase are strongly correlated: large positive and negative values of the phase derivative coincide with the zeroes or near-zeroes of the amplitude. This indicates that, as one crosses over from one speckle to a neighboring speckle in the frequency domain, a phase jump is encountered.

The complex field transmission coefficient $t_{ab}(\omega)$ in Fig. 15 can be autocorrelated and averaged together with data from the other speckles. The result is proportional to the field autocorrelation function $C_E(\triangle\omega)$. Similarly, the intensity autocorrelation function $C_I(\triangle\omega)$ can be found by autocorrelating $|t_{ab}(\omega)|^2$. The results are shown in Fig. 16. The data should be compared with the theoretical results [33]

$$C_E(\triangle\omega) = Re\left(\frac{q(L + z_1 + z_2)}{\sinh(q(L + z_1 + z_2))}\right), \tag{15}$$

$$C_I(\triangle\omega) = \left|\frac{q(L + z_1 + z_2)}{\sinh(q(L + z_1 + z_2))}\right|^2, \tag{16}$$

where $q = \sqrt{2\triangle\omega/D}$. The agreement is excellent at low frequency shifts, but deviations appear at larger shifts due to the limited number of speckles. From the fits, the value $D = 21$ m^2/s is found, as before. It should be noted that Eq. 16 is only the highest order term in the intensity correlations. Other terms contain the long range fluctuations and the universal conductance

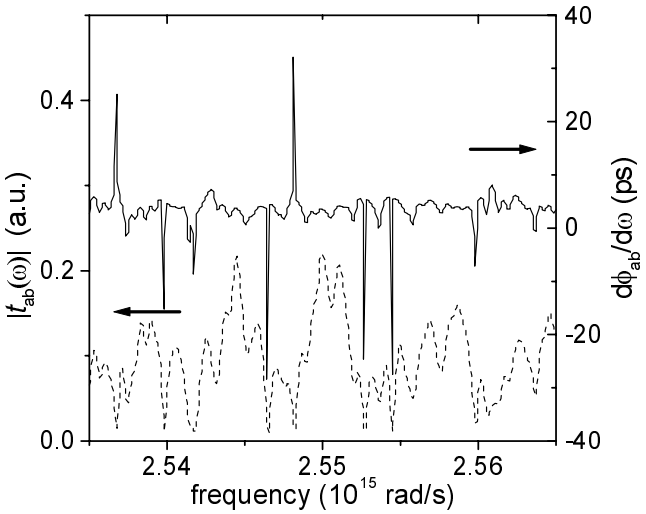

Figure 15. Modulus (dashed line, left scale) and phase derivative (full line, right scale) of t_{ab} measured on a sample of A-GaP of $L = 15$ μm.

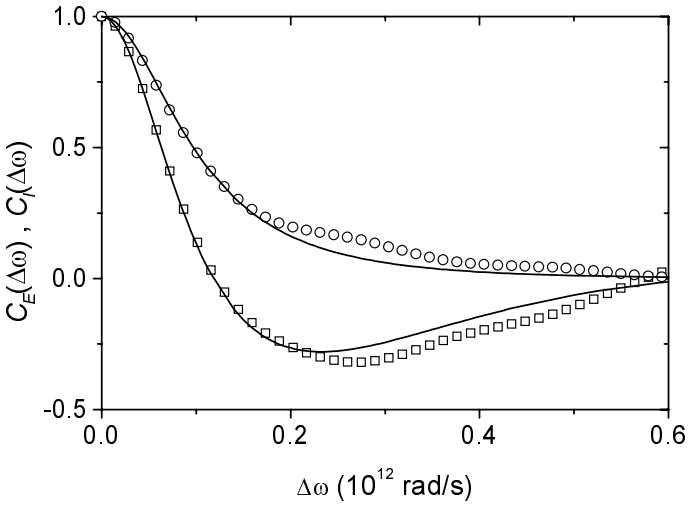

Figure 16. Field (squares) and intensity (circles) correlation functions measured on the sample of Fig. 15. The lines are Eqs. 15 and 16 with $D = 21$ m^2/s.

fluctuations which have an amplitude of $1/g$ and $1/g^2$, respectively, where g is the dimensionless conductance. In this experiment g is estimated to be on the order of 100, so that the extra terms are expected to be small.

Using the ensemble of data from all measured speckles over the whole frequency content of the laser pulse the distributions of the amplitude and phase can be studied. The complex field measured in a speckle is the sum of random contributions from partial waves traversing every possible path through the sample. This sum therefore represents a random walk in the complex plane. By the central limit theorem the real (r) and imaginary (i) parts of the measured field, and thus of t_{ab}, must then have a Gaussian distribution:

$$P(r,i) = \frac{1}{2\pi\sigma^2} \exp(-\frac{r^2+i^2}{2\sigma^2}) \tag{17}$$

The measured distributions are shown in Fig. 17. To remove the instrumental response the real and imaginary parts of t_{ab} have been normalized by the ensemble average of the modulus $|t_{ab}| = (r^2+i^2)^{1/2}$. The Gaussian distribution provides a very good fit. There was no correlation between r and i: $\langle ri \rangle = 0$. The parameter σ was found to be 0.793, close to the expected value of $\sqrt{2/\pi}$. The phase ϕ_{ab} is seen to be evenly distributed over 2π, as expected.

In Fig. 18 the distribution of $\phi' = d\phi_{ab}/d\omega$ is shown. The data for different sample thicknesses collapse onto a single distribution after normalizing ϕ' to its ensemble average $\langle \phi' \rangle$. Recently, this distribution was also measured for transmission of microwaves through random waveguides [34]. The microwave data were found to be described well by the theoretical distribution

$$P(\phi') = \frac{1}{2} \frac{Q}{(Q + (\phi' / \langle \phi' \rangle - 1)^2)^{3/2}}. \tag{18}$$

Here Q is a function of L/L_a which equals 0.4 in the limit $L_a \to \infty$ and is smaller otherwise [35]. This distribution is seen to describe the experimental distribution very well for all sample thicknesses. From the fit we find $Q = 0.43 \pm 0.05$, as expected for nonabsorbing samples.

We have shown that ultrashort pulse interferometry greatly increases the amount of dynamical information that one can obtain on the propagation of light in strongly scattering samples. Deviations from diffusion theory are expected to show up in the measured quantities as the localization threshold is approached. In the present samples of anodically etched GaP all the data can still be described completely with diffusion theory.

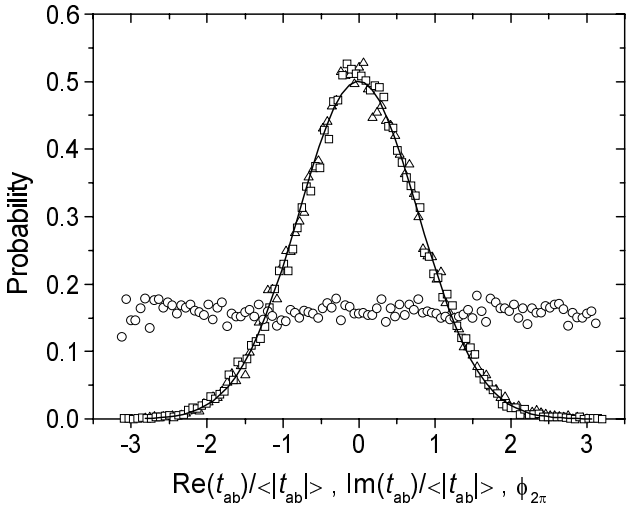

Figure 17. Probability distribution function of the real (triangles) and imaginary (squares) parts of the field transmission coefficient t_{ab} and of its phase modulo 2π (circles). The full line is a Gaussian fit.

5. Conclusion

In conclusion, disordered semiconductor samples based on powders of Si, Ge, GaAs, and macroporous GaP display many effects that are associated with strongly multiple scattering of light. A combination of careful static and dynamic measurements on a range of sample thicknesses is necessary to fully characterize the optical transport. All the semiconductor samples we studied have kl_s values that are in the range of strong localization effects, assuming that the precise location of the transition is determined by kl_s of order 1. The exact position of the localization transition and the behavior at the transition is still pendent and may depend on other sample characteristics such as powder size distribution and topology, residual absorption, boundary reflection associated with the effective refractive index of the sample and finite sample size effects. The scaling behavior of dynamical quantities associated with the diffusion constant and the energy velocity in systems near localization may differ considerably from the static properties such as the kl_s product. For example, recent theoretical work indicated that the mean free path near localization is position dependent and gradually changes from the smallest value in the bulk to larger values near the edges of the sample [27]. Further study on e.g. monodisperse powders and other

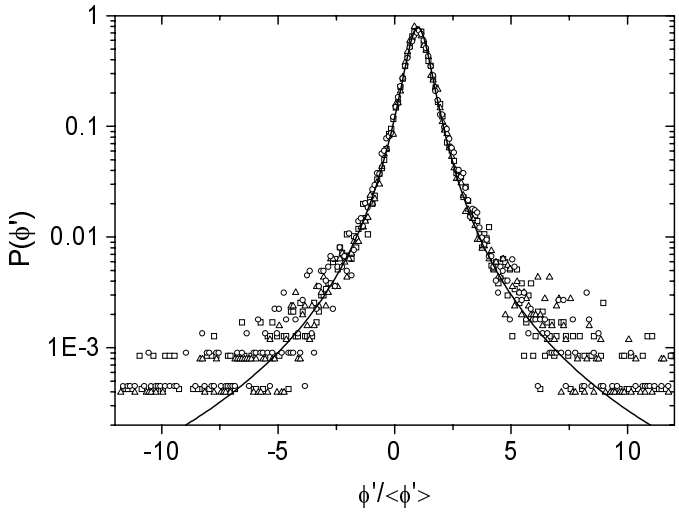

Figure 18. Probability distribution of the phase derivative for sample thickness L =5 (triangles), 10 (circles), and 18 (squares) μm. The full line is Eq. 18 with $Q = 0.4$.

topologically well-defined samples is necessary to uncover the localization behavior in these strongly scattering systems.

6. Acknowledgments

We are inbdeted to D. Vanmaekelbergh and J. van de Lagemaat for preparing the GaP samples, to C.M. Soukoulis and K. Busch for the EDCPA calculations, and to L.D. Noordam and C.W. Rella for their collaboration with the work done on Ge samples. We gratefully acknowledge P. de Vries, R. H. J. Kop, D. S. Wiersma, W. L. Vos, H. P. Schriemer, M. Megens, Duong Dau, G. van Soest, and Gerard Wegdam for fruitful discussions and contributions. Financial support has been supplied for JGR by the European Commission through Grant No. ERBFM- BICT971921. This work is part of the research program of the Stichting voor Fundamenteel Onderzoek der Materie, which is financially supported by the Nederlands Organisatie voor Wetenschappelijk Onderzoek.

References

1. P. Sheng, *Introduction to Wave Scattering, Localization, and Mesoscopic Phenomena*, (Academic Press, New York) 1995.

2. M.P. van Albada, A. Lagendijk, Phys. Rev. Lett. 55: 2692 (1985); P.E. Wolf, G. Maret, Phys. Rev. Lett. 55: 2696 (1985).
3. 'Photonic Band Gaps and Localization', NATO ASI B 308, Edited by C.M. Soukoulis. Proc. of ARW, Heraklion, Crete (Greece), 1992, Kluwer (1993).
4. 'Advances in Optical Imaging and Photon Migration 1998', Edited by James G. Fujimoto and Michael S. Patterson, Trends in Optics and Photonics Series, Vol. 21, OSA (1998).
5. P.W. Anderson, Phys. Rev. 109: 1492 (1958).
6. S. John, Phys. Rev. Lett. 53: 2169 (1984); P.W. Anderson, Philos. Mag. B 52: 505 (1985).
7. A.F. Ioffe and A.R. Regel, Prog. Semicond. 4: 237 (1960).
8. N. Garcia and A.Z. Genack, Phys. Rev. Lett. 66: 1850 (1991).
9. D.S. Wiersma, P. Bartolini, A. Lagendijk, and R. Righini, Nature 390: 671 (1997).
10. F. Scheffold, R. Lenke, R. Tweer, and G. Maret, Nature 398: 206 (1999).
11. J. Gómez Rivas, R. Sprik, C.M. Soukoulis, K. Busch, and A. Lagendijk, Europhys. Lett. 48: 22 (1999).
12. F.J.P. Schuurmans, D. Vanmaekelbergh, J. van de Lagemaat, and A. Lagendijk, Science 284: 141 (1999).
13. F.J.P. Schuurmans, M. Megens, D. Vanmaekelbergh, and A. Lagendijk, Phys. Rev. Lett. 83: 2183 (1999).
14. A.Z. Genack, Phys. Rev. Lett. 58: 2043 (1987).
15. M.P. van Albada, B.A. van Tiggelen, A. Lagendijk, and A. Tip, Phys. Rev. Lett. 66: 3132 (1991).
16. R. H. J. Kop, P. de Vries, R. Sprik, and A. Lagendijk, Phys. Rev. Lett. 79: 4369 (1997).
17. A. Kirchner, K. Busch and C.M. Soukoulis, Phys. Rev. B 57: 277 (1998).
18. A. Ishimaru, *Wave Propagation and Scattering in Random Media* (Academic Press, New York, 1995).
19. A. Lagendijk, R. Vreeker, and P. de Vries, Phys. Lett. A 136: 81 (1989).
20. J.X. Zhu, D.J. Pine, and D.A. Weitz, Phys. Rev. A 44: 3948 (1991).
21. E. Abrahams, P.W. Anderson, D.C. Licciardello, and T.V. Ramakrishnan, Phys. Rev. Lett. 42: 673 (1979).
22. M.U. Vera and D.J. Durian, Phys. Rev. B 53: 3215 (1996).
23. S. Datta, C.T. Chan, K.M. Ho, and C.M. Soukoulis, Phys. Rev. B 48: 14936 (1993).
24. J. Gómez Rivas, R. Sprik, A. Lagendijk, L.D. Noordam, and C.W. Rella, accepted for publication in Phys. Rev. E RC.
25. K. Busch and C.M. Soukoulis, Phys. Rev. Lett. 75: 3442 (1995); A. Kirchner, K. Busch, and C.M. Soukoulis, Phys. Rev. B 49: 3800 (1994).
26. D.S. Wiersma, M.P. van Albada, and A. Lagendijk, Rev. Sci. Instruments. 66: 5473 (1995).
27. B.A. Tiggelen, A. Lagendijk, and D.S. Wiersma, Phys. Rev. Lett. 84: 4333 (2000).
28. J. Gómez Rivas, R. Sprik, and A. Lagendijk, Ann. Phys. (Leipzig) 8: 77 (1999) Spec. Issue.
29. R. H. J. Kop and R. Sprik, Rev. Sci. Instrum. 66: 5459 (1995).
30. S. John, Phys. Rev. Lett. 58: 2486 (1987).
31. A. Z. Genack and J. M. Drake, Europhys. Lett. 11: 331 (1990).
32. A. Imhof, W. L. Vos, R. Sprik, and A. Lagendijk, Phys. Rev. Lett. 83: 2942 (1999).
33. S. Feng, C. Kane, P. A. Lee, and A. D. Stone, Phys. Rev. Lett. 61: 834 (1988).
34. A. Z. Genack, P. Sebbah, M. Stoytchev, and B. A. van Tiggelen, Phys. Rev. Lett. 82: 715 (1999).
35. B. A. van Tiggelen, P. Sebbah, M. Stoytchev, and A. Z. Genack, Phys. Rev. E **59**, 7166 (1999).